ELSEVIER

Journal of Computational and Applied Mathematics 109 (1999) 95–122

JOURNAL OF COMPUTATIONAL AND APPLIED MATHEMATICS

Discrete variable and finite element techniques applied to simple atomic systems

W. Schweizer[a, *], P. Faßbinder[a], R. González-Ferez[b], M. Braun[c], S. Kulla[a], M. Stehle[a]

[a] *Institut für Theoretische Astrophysik, Universität Tübingen, Auf der Morgenstelle 10, 72076 Tübingen, Germany*

[b] *Instituto "Carlos I" de Fisica Teorica y Computacional, Universidad de Granada, E-18071 Granada, Spain*

[c] *Physics Department, University of South Africa, P.O.Box 392, 0003 Pretoria, South Africa*

Received 14 April 1998

Abstract

We present effective numerical algorithms based on discrete variable techniques and finite elements for solving the non-separable three-dimensional Schrödinger equation and a method for the solution of the two electron problem in a strong magnetic field, that combines the hyperspherical close coupling and the Finite Element method. As an example we will present some atomic data for the hydrogen and the helium atom in external fields relevant for magnetic white dwarf stars.

Keywords: Discrete variable method; Finite element method; Complex coordinate rotation; Non-integrable systems; Alkali metal atoms; Helium atom; Resonances

1. Introduction

In this paper we will describe some modern numerical methods recently developed and applied to simple atomic systems. A simple atomic system is an atom or ion, which can be accurately described by an effective one- or two-particle Hamiltonian. But note, the numerical methods presented in this paper are not only restricted to atomic systems. These numerical techniques are also useful for computations with respect to other simple quantum systems, e.g., in solid-state physics shallow donor states in GaAs [19] are accurately described by an Hamiltonian equivalent to the hydrogen atom, in nuclear physics giant resonances in closed-shell nuclei can be treated by phenomenological one-particle interactions like the Brink–Boeker or Skyrme interactions [28], in quest of quantumchaology non-integrable single-particle Hamiltonians are of importance, and so forth. The

* Corresponding author.

E-mail address: schweize@tat.physik.uni.tuebingen.de (W. Schweizer)

0377-0427/99/$ - see front matter
PII: S0377-0427(99)00155-7

applications presented in this paper are restricted to hydrogen atoms in external and van-der-Waals fields, alkali metal atoms and alkali-like ions in external fields, wave-packet problems and the helium atom and helium isoelectronic sequence in strong magnetic fields. Interpreting observations from magnetic white dwarfs, neutron stars and Am-Hercules systems necessitate the knowledge of the relevant atomic data, hence transition wave lengths and rates of hydrogen, helium and some alkali ions in strong magnetic and electric fields have to be computed.

Simple quantum system does not mean that computations are simple. E.g., magnetic white dwarfs and neutron stars possess magnetic fields of the order of 10^2–10^5, and 10^7–10^9 T, respectively. At these extremely high field strengths the Lorentz force acting on an atomic electron equals or exceeds the Coulomb binding force, even for low-lying states. Due to the different symmetry of the Coulomb and the Lorentz interaction the system is no longer quantum integrable. Thus it is evident that perturbation theory is no longer applicable and more refined numerical methods become necessary.

Integrability of a n-dimensional Hamiltonian system requires the existence of n commuting observables O_i, $1 \leqslant i \leqslant n$. Each separable system is integrable, but not vice versa. Observables are given by hermitian operators and their eigenvalues can serve as quantum-labels for the wave functions. For separable systems the eigenvalues (separation constants) of each of the three (in general n) unidimensional differential equations can be used to label the eigenfunctions $\psi(\boldsymbol{r})$ and hence serve as quantum numbers. For a three-dimensional system it can be shown that the Laplace–Beltrami operator Δ can be separated in exactly 11 different curvilinear [24] coordinates. For each of these coordinates the potential $V(\boldsymbol{r})$ has to fulfil certain properties, that the Schrödinger equation

$$\left[-\frac{\hbar^2}{2m}\Delta + V(\boldsymbol{r})\right]\psi_E(\boldsymbol{r}) = E\psi_E(\boldsymbol{r}) \tag{1}$$

becomes separable. For all orthogonal curvilinear coordinates q_j in three dimensions the following conditions hold:

$$\mathrm{d}s^2 = \mathrm{d}x^2 + \mathrm{d}y^2 + \mathrm{d}z^2$$

with (x, y, z) cartesian coordinates,

$$\mathrm{d}s^2 = \sum_{i,j=1}^{3} g_{ij}\,\mathrm{d}q_i\,\mathrm{d}q_j \quad \text{and} \quad g_{ij} = \delta_{ij}g_{ii},$$

$$\Delta_{q1,q2,q3} = \frac{1}{\sqrt{g}}\sum_{i=1}^{3}\frac{\partial}{\partial q_i}\left(\frac{\sqrt{g}}{g_{ii}}\frac{\partial}{\partial q_i}\right) \quad \text{(Laplace–Beltrami operator)},$$

$$\mathrm{d}V = \sqrt{g}\,\mathrm{d}q_1\,\mathrm{d}q_2\,\mathrm{d}q_3 \quad \text{(volume element)} \tag{2}$$

with $g = g_{11}g_{22}g_{33}$, and the quantum system becomes separable, if the potential can be written as

$$V(q_1, q_2, q_3) = \sum_{i=1}^{3}\frac{1}{g_{ii}}V(q_i). \tag{3}$$

Using Eq. (3) it can be easily proved if and for which coordinates a given one-particle quantum system is separable.

In Section 2 we will present some numerical methods useful for non-separable quantum systems. First we will discuss the discrete variable method followed by the finite element method and in Section 2.3 a combination of hyperspherical closed coupling and finite element techniques, useful for two-electron systems. All these methods lead to an Hamiltonian matrix and hence to a generalized eigenvalue problem. In Section 2.4 we will briefly discuss techniques for computing eigenenergies and eigenstates from the already derived Hamiltonian matrix. In Section 3 we will present some results for the hydrogen atom in external fields, we will discuss resonances, model potential techniques useful to obtain atomic data from alkali-metal atoms and alkali-like ions in external fields, and finally the helium atom in a strong magnetic field. The paper will be completed by Section 4 with a discussion and an outlook on future work.

2. Methods

In this Section we will first describe the discrete variable method for three-dimensional nonrelativistic quantum systems followed by a discussion of the finite element method. Higher n-dimensional systems could be expanded by, e.g., n-dimensional finite elements. However, for many physical systems it turns out that it is numerically more promising to combine finite elements of lower dimensions with certain basis function expansions. This is especially the case if non-Euclidean coordinates are used. Sparse grid techniques for higher dimensions are only available for Euclidean coordinate systems. This section will be completed by some remarks about diagonalization routines.

2.1. The discrete variable technique

The motivation for using the discrete variable method [21] in our approach is to transform the three-dimensional Schrödinger equation into a system of coupled uni-dimensional differential equations. To derive the differential system, the Hamiltonian is expanded with respect to the discretized eigensolution of a suitable operator, which we choose as the angular momentum operator. But note, this expansion is not justified by a certain approximate symmetry of the system under consideration, it is a numerical way to optimize the computation. The resulting coupled ordinary differential equations will then be solved by finite elements. By this method we were able to obtain solutions for the hydrogen atom in parallel electric and magnetic fields on workstations for field strengths and energy values for which Hamiltonian expansions based on Sturmians [39] did not even converge on supercomputers.

By using appropriate units ($\hbar = 1$, $m_e = 1$) and spherical coordinates the one-particle Hamiltonian becomes

$$H(r,\theta,\phi) = -\frac{1}{2r^2}\frac{\partial}{\partial r}r^2\frac{\partial}{\partial r} + \frac{1}{2r^2}L^2(\theta,\phi) - \mathrm{i}\beta\frac{\partial}{\partial\phi} + V(r,\theta,\phi), \tag{4}$$

where

$$L^2(\theta,\phi) = -\frac{1}{\sin\theta}\left(\frac{\partial}{\partial\theta}\sin\theta\frac{\partial}{\partial\theta} + \frac{1}{\sin\theta}\frac{\partial^2}{\partial\phi^2}\right) \tag{5}$$

and the derivation operator $\mathrm{i}\frac{\partial}{\partial\phi} = L_z$ is already included to describe additional external magnetic fields with field strength β. A complete set of orthonormal eigenfunctions of the angular momentum

operator L^2 (5) is given by

$$\chi_v(\Omega) = \frac{1}{C_v} P_l^m(\cos\theta) \begin{cases} \cos m\phi & \text{for } m \geqslant 0, \\ \sin |m|\phi & \text{for } m < 0, \end{cases} \tag{6}$$

where $\Omega = \{\theta, \phi\}$, P_l^m the associated Legendre functions,

$$C_v = \sqrt{2\pi \frac{1+\delta_{0m}}{2l+1} \frac{(l+|m|)!}{(l-|m|)!}} \tag{7}$$

and

$$L^2 \chi_v = \lambda_v \chi_v, \quad \lambda_v = l(l+1) \quad \text{with } v = \{l, m\}. \tag{8}$$

The two-dimensional subspace Ω is discretized via a difference grid with N nodal points Ω_k:

$$\Omega \to \Omega_k = \{\theta_k, \phi_k\}, \tag{9}$$

$$\psi(r, \Omega) \to \psi(r, \Omega_k) = \psi_k(r) + \mathrm{i}\tilde{\psi}_k(r), \tag{10}$$

where $\psi_k(r)$ and $\tilde{\psi}_k(r)$ are real scalar functions.

One important computational aspect is the optimal choice for the nodal points. Let us first consider the two-dimensional case in which the magnetic quantum number m is conserved. This holds for systems with cylindrical symmetry with respect to the z-axis, e.g. for alkali-metal atoms in parallel electric and magnetic fields. Up to normalization constants the eigenfunctions, Eq. (6), are then reduced to the associated Legendre polynomials, and only the angular coordinate θ has to be discretized. The associated Legendre polynomials are orthogonal polynomials [35]. Hence by taking the N nodal points θ_k at the zeros of the Legendre polynomial $P_{N+m}^m(x)$ in the interval $x \in [-1, 1]$, a set of orthogonal vectors $\{P_l^m(\cos\theta_k), m \leqslant l \leqslant (N-1+m)\}$ is defined. By taking these set of orthogonal vectors a square matrix χ could be constructed which becomes together with a suitable normalization constant orthogonal and hence its inverse is simply given by transposing. Note that the corresponding Gauss–Legendre quadratures are exact, which is not true in general. For three dimensions we design a N^2 grid by choosing N nodal points with respect to θ as described above and, for the variable Φ, N equidistant nodal points in the interval $[0, 2\pi]$. Taking the value of the first N^2 nodal points Ω_k as defined above, the square matrix χ becomes

$$\chi_{kv} = \chi_v(\Omega_k) \tag{11}$$

and its inverse χ^{-1} can be constructed. Thus the wave function can be expanded in terms of the matrix χ:

$$\psi(r, \Omega) = \sum_{k=1}^{N^2} \left(\sum_{v=1}^{N^2} \chi_v(\Omega) \chi_{vk}^{-1} \right) (\psi_k(r) + \mathrm{i}\tilde{\psi}_k(r)). \tag{12}$$

This expansion has the advantage, that all those parts in the Hamiltonian become diagonal which are independent of angular derivative operators. In order to keep the Hamiltonian matrix symmetric we have to introduce a normalization condition for the radial function Eq. (10)

$$1 = \sum_{k,j=1}^{N^2} \left(\sum_{v=1}^{N^2} \chi_{vk}^{-1} \chi_{vj}^{-1} \right) \int_0^\infty \mathrm{d}r r^2 [\psi_k(r)\psi_j(r) + \tilde{\psi}_k(r)\tilde{\psi}_j(r)]. \tag{13}$$

Inserting the expansion, Eq. (12), into the Schrödinger equation (4) at the nodal points Ω_k together with the normalization condition (13) leads to a system of $2N^2$ coupled uni-dimensional differential equations for the radial functions $\psi_k(r)$ and $\tilde{\psi}_k(r)$:

$$0 = \sum_{j=1}^{N^2} [(d_{kj}(r) + v_{kj}(r))\psi_j(r) + \tilde{v}_{kj}(r)\tilde{\psi}_j(r)], \tag{14}$$

$$0 = \sum_{j=1}^{N^2} [(d_{kj}(r) + v_{kj}(r))\tilde{\psi}_j(r) - \tilde{v}_{kj}(r)\psi_j(r)], \tag{15}$$

where

$$d_{kj}(r) = \left\{ -\frac{1}{2r^2}\frac{\mathrm{d}}{\mathrm{d}r}r^2\frac{\mathrm{d}}{\mathrm{d}r} + V(r,\Omega_j) - E \right\} g_{kj}, \tag{16}$$

with

$$g_{kj} = \sum_{v=1}^{N^2} \chi_{vk}^{-1}\chi_{vj}^{-1} \tag{17}$$

and

$$v_{kj}(r) = \frac{1}{2r^2}\sum_{v=1}^{N^2} \lambda_v \chi_{vk}^{-1}\chi_{vj}^{-1}, \tag{18}$$

$$\tilde{v}_{kj}(r) = \beta \sum_{v=1}^{N^2} m\chi_{vk}^{-1}\chi_{-vj}^{-1}, \quad -v = \{l, -m\}. \tag{19}$$

Note, that for either vanishing coefficients β in the Hamiltonian or for Hamiltonians' (4) separable with respect to ϕ the radial expansion becomes real and hence $\tilde{\psi}_k(r) = 0$.

The remaining task is to solve this system of coupled differential equations. By applying the finite element method we arrive at a banded symmetric Hamiltonian matrix which we solve using a spectral transformation Lanczos method. For Coulomb-like potentials it turns out that the finite element computations in the radial coordinate are optimized by quadratically spaced nodal points

$$r_i = \frac{(i-1)^2}{M^2} r_{\max}, \quad i = 1 \cdots M \tag{20}$$

as described in the following section.

2.2. The finite element method

In this section we will describe the basic idea of the finite element method and hence restrict our discussion for simplicity to uni-dimensional systems and bound states. Generalizations with respect to both, higher dimensions and nonbound states will be discussed in the following sections.

In the discrete variable method the space is discretized but the expansion polynomials are still globally defined functions. Therefore the discrete variable technique is a kind of hybrid method between the finite element or finite difference methods and the techniques based on global basis

expansions. In the finite element methods not only the space will be discretized into local elements, the approximation polynomials are in addition only defined on this local element. Therefore, we are able to change not only the size of the finite elements but in addition the locally selected basis in type and order. Usually only the size of the local element is changed from element to element but the type and order of the approximation polynomials is kept fixed.

Starting point of the discussion is the one-dimensional Schrödinger equation

$$\left\{-\frac{\hbar^2}{2m}\frac{\mathrm{d}^2}{\mathrm{d}x^2}+(E-V(x))\right\}\psi_E(x)=0. \tag{21}$$

Finite element techniques can be applied to any differential equation, not necessarily of Schrödinger type. Note, that due to the potential function it is not simple to find an alternative description in momentum space. Therefore, finite element techniques are usually formulated in coordinate space. For simplification we set

$$\hbar=1, \quad m=\frac{1}{2} \quad \Rightarrow \frac{\hbar^2}{2m}=1. \tag{22}$$

As bound states $\langle x|\psi\rangle=\psi(x)$ are normalizable we could always find a left and right border, (x_a,x_b), in space beyond which the wave functions effectively vanish:

$$\langle x_a|\psi\rangle=0=\langle x_b|\psi\rangle. \tag{23}$$

By multiplication of the Schrödinger equation with the wave function $\psi(x)$ from the left we arrive at an equivalent integral equation

$$\int_{-\infty}^{+\infty}\left[\psi(x)\frac{\mathrm{d}^2}{\mathrm{d}x^2}\psi(x)+\psi(x)(E-V(x))\psi(x)\right]\mathrm{d}x=0, \tag{24}$$

which by partial integration gives

$$\begin{aligned}&\int_{x_a}^{x_b}\left[\underbrace{\psi(x)\frac{\mathrm{d}^2}{\mathrm{d}x^2}\psi(x)}+\psi(x)(E-V(x))\psi(x)\right]\mathrm{d}x=0,\\ &=\underbrace{\psi(x)\frac{\mathrm{d}}{\mathrm{d}x}\psi(x)\Big|_{x_a}^{x_b}}_{\text{at the border}=0}-\int_{x_a}^{x_b}\left[\frac{\mathrm{d}}{\mathrm{d}x}\psi(x)\right]^2\mathrm{d}x.\end{aligned} \tag{25}$$

This integral equation can be formulated as a functional of the wave function ψ

$$I[\psi]=-\int_{x_a}^{x_b}\left[\frac{\mathrm{d}}{\mathrm{d}x}\psi(x)\right]^2\mathrm{d}x+\int_{x_a}^{x_b}\psi(x)\underbrace{[E-V(x)]}_{\sigma(x)}\psi(x)\,\mathrm{d}x \tag{26}$$

and by the following expansion:

$$\psi(x)=\sum_i C_i N_i(x), \tag{27}$$

we arrive finally at

$$I[\psi]=\sum_{i,j}C_iC_j\int\left[N_i(x)\sigma(x)N_j(x)-\frac{\mathrm{d}}{\mathrm{d}x}N_i(x)\frac{\mathrm{d}}{\mathrm{d}x}N_j(x)\right]\mathrm{d}x. \tag{28}$$

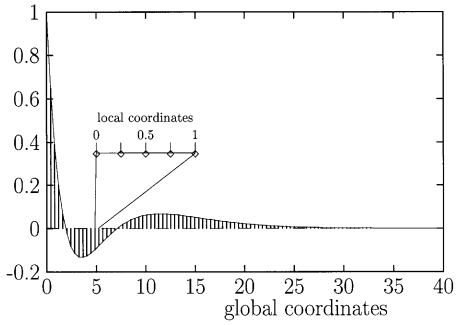

Fig. 1. Graphical picture of a wave function in the local basis. The entire space is divided into small elements. On each of the locale elements the wave function is expanded with respect to the interpolation polynomial. In this example each element has five nodal points at 0, 0.25, 0.5, 0.75 and 1. The first and the last nodes are always common with the neighbouring element.

Up to now the basis functions $N_i(x)$ are still arbitrary and not restricted to a finite element approach. In the finite element frame a suitable approximation is given by Lagrange- or Hermite-interpolation polynomials.

As already mentioned above, the entire space will be divided in small pieces, the elements. On each of this elements we define a local basis, the nodal point coordinates:

$$r = r_0^{(n-1)} + h^{(n)} \underbrace{x}_{\text{loc. coord.}}, \tag{29}$$

$$x = 0 \cdots 1,$$

$$r = r_0^{(n-1)} \cdots r_0^{(n)} + h^{(n)} = r_0^{(n)}$$

with $h^{(n)}$ the length of the nth finite element, $r_0^{(n-1)}$ the global position in space of the left-hand border of the element and x the local coordinate. In Fig. 1 a simple example with constant finite elements is shown.

For finite elements of constant dimension the following properties hold:

$$r_0^{(n-1)} = (n-1)h, \quad h^{(n)} = h \quad \forall n \in N. \tag{30}$$

A quadratic spacing is numerically more favourable for Coulomb systems:

$$r_0^{(n-1)} = (n-1)^2 h_0 \quad n = 1, \ldots, n_{\max}, \tag{31}$$

and hence the size of the elements increases linearly

$$h^{(i)} = r_0^{(i+1)} - r_0^{(i)} = (2i+1)h_0 \qquad n = 1, \ldots, n_{\max} - 1. \tag{32}$$

Of course, the optimal spacing depends on the physical system under consideration. E.g., for a parabolic potential (harmonic oscillator) a constant spacing is numerically favoured. The wave function is given by

$$\psi(r) = \sum_{\alpha} \underbrace{\Phi_\alpha(x)}_{\text{interpol. basis}} \cdot \psi_\alpha^{(n)} \quad r \in]r_0^{(n-1)}, r_0^{(n-1)} + h^{(n)}[, \tag{33}$$

where $\psi_\alpha^{(n)}$ is the correct value of the wave function at the nodal points and the summation α runs over all interpolation polynomials.

Common interpolation polynomials are the Lagrange, the Hermitian and the extended Hermitian interpolation polynomials. (Unfortunately this interpolation polynomials are often simply called Lagrangian and Hermitian which should not be mixed up with the polynomial functions of the same name.) Let us first discuss in more detail Lagrange interpolation polynomials, labelled by the index α. In the following discussion, we assume that the whole space of interest $[x_a, x_b]$ is divided in smaller elements carrying a local coordinate system $\tilde{x}$ running from $[-1, +1]$.

In the selected interpolation the wave function is given by

$$\psi(\tilde{x}) = \sum_\alpha \Phi_\alpha(\tilde{x})\psi(\tilde{x}_\alpha) = \sum_\alpha \underbrace{\Phi_\alpha(\tilde{x})}_{\text{inter. polynom}} \psi_\alpha, \tag{34}$$

thus if the interpolation polynom satisfies

$$\Phi_\alpha(\tilde{x}_\beta) = \delta_{\alpha,\beta}, \tag{35}$$

the wave function $\psi(x)$ will have its correct values at the nodes $\tilde{x}_\alpha$.

A polynomial of order n has $n+1$ linear independent coefficients $C_{\alpha i}$ and hence $n+1$ nodal points in $-1 \leqslant \tilde{x} \leqslant +1$ which are equidistantly distributed. E.g. for three nodes we get $n=2$, $\tilde{x}_0 = -1$, $\tilde{x}_1 = 0$, $\tilde{x}_2 = +1$ and hence a system of linear equations

$$\begin{aligned}
&\Phi_0(\tilde{x}_0) = \Phi_0(-1) = C_{00} - C_{01} + C_{02} = 1,\\
&\Phi_0(\tilde{x}_1) = \Phi_0(0) = C_{00} = 0,\\
&\Phi_0(\tilde{x}_2) = \Phi_0(+1) = C_{00} + C_{01} + C_{02} = 0
\end{aligned}$$

and similar additional equations for Φ_1 and Φ_2. This linear system of equation can be condensed to a matrix equation

$$\begin{pmatrix} 1 & -1 & 1 \\ 1 & 0 & 0 \\ 1 & 1 & 1 \end{pmatrix} \cdot \begin{pmatrix} C_{00} & C_{10} & C_{20} \\ C_{01} & C_{11} & C_{21} \\ C_{02} & C_{12} & C_{22} \end{pmatrix} = \begin{pmatrix} 1 & 0 & 0 \\ 0 & 1 & 0 \\ 0 & 0 & 1 \end{pmatrix}, \tag{36}$$

whose solution will give the unknown coefficients $C_{\alpha i}$ for our Lagrange interpolation polynomial. Generalized for a polynomial of arbitrary order we get the following linear equation:

$$\underbrace{A}_{\text{nodes}} \cdot \underbrace{C}_{\text{coefficient matrix}} = \underbrace{\mathbf{1}}_{\text{unity matrix}} \Rightarrow C = A^{-1}, \tag{37}$$

by which we can easily compute the unknown coefficients of the Lagrangian interpolation polynomial.

In addition to the equidistant distribution of the nodal points the Lagrange interpolation polynomial are defined via the wave function not taking into account its derivative. Hermitian interpolation polynomials are in addition defined by the assumption that value and derivation of the wave function are correct at the nodal points. Hence we get the following ansatz:

$$\begin{aligned}
\psi(\tilde{x}) &= \sum_\alpha \left(\Phi_\alpha(\tilde{x})\psi(\tilde{x}_\alpha) + \bar{\Phi}_\alpha(\tilde{x}) \frac{\mathrm{d}}{\mathrm{d}\tilde{x}} \psi(\tilde{x}_\alpha) \right)\\
&= \sum_\alpha (\Phi_\alpha(\tilde{x})\psi_\alpha + \bar{\Phi}_\alpha(\tilde{x})\bar{\psi}_\alpha)
\end{aligned} \tag{38}$$

and for the derivative of the wave function $\psi'(\tilde{x})$

$$\psi'(\tilde{x}) = \sum_{\alpha}(\Phi'_{\alpha}(\tilde{x})\psi_{\alpha} +' \bar{\Phi}_{\alpha}(\tilde{x})\bar{\psi}_{\alpha}), \tag{39}$$

which leads to

$$\begin{aligned} &\Phi_{\alpha}(\tilde{x}_{\beta}) = \delta_{\alpha\beta} \Rightarrow \text{for } n \text{ nodes } n \text{ equations,} \\ &\frac{\mathrm{d}}{\mathrm{d}\tilde{x}}\bar{\Phi}_{\alpha}(\tilde{x}_{\beta}) = \delta_{\alpha\beta} \Rightarrow \text{for } n \text{ nodes } n \text{ equations,} \end{aligned} \tag{40}$$

hence n nodal points lead to a total of $2n$ linear equations and thus a polynomial of order $2n-1$.

The next interpolation step are extended Hermitian polynomials in which not only the wave function and its derivative but in addition its second derivative are taken into account. Hence we get

$$\begin{aligned} \psi(\tilde{x}) &= \sum_{\alpha}\left(\Phi_{\alpha}(\tilde{x})\psi(\tilde{x}_{\alpha}) + \bar{\Phi}_{\alpha}(\tilde{x})\frac{\mathrm{d}}{\mathrm{d}\tilde{x}}\psi(\tilde{x}_{\alpha}) + \bar{\bar{\Phi}}_{\alpha}(\tilde{x})\frac{\mathrm{d}^2}{\mathrm{d}\tilde{x}^2}\psi(\tilde{x}_{\alpha})\right) \\ &= \sum_{\alpha}(\Phi_{\alpha}(\tilde{x})\psi_{\alpha} + \bar{\Phi}_{\alpha}(\tilde{x})\bar{\psi}_{\alpha} + \bar{\bar{\Phi}}_{\alpha}(\tilde{x})\bar{\bar{\psi}}_{\alpha}) \end{aligned} \tag{41}$$

and therefore the polynomials have to fulfil

$$\begin{aligned} \Phi_{\alpha}(\tilde{x}_{\beta}) &= \delta_{\alpha\beta}, \\ \frac{\mathrm{d}}{\mathrm{d}\tilde{x}}\bar{\Phi}_{\alpha}(\tilde{x}_{\beta}) &= \delta_{\alpha\beta}, \\ \frac{\mathrm{d}^2}{\mathrm{d}\tilde{x}^2}\bar{\bar{\Phi}}_{\alpha}(\tilde{x}_{\beta}) &= \delta_{\alpha\beta}. \end{aligned} \tag{42}$$

For n nodal points a complete description will be given by $3n$ coefficients and hence the corresponding polynomial is of the order $3n-1$. All further derivations are equivalent to those described in detail for Lagrangian interpolation polynomials and therefore are omitted. (A simple MAPLE program is available on request for solving the corresponding linear equations for these three types of interpolation polynomials and a further MAPLE program for one-dimensional finite element computations, thought as a rather pedagogical tool. A very nicely and pedagogically written paper about using the finite element method for the hydrogen atom in strong magnetic fields is [27].)

2.3. The finite element technique applied to helium in a strong magnetic field

Three-body Coulomb systems in quantum mechanics are of principal interest due to its fundamental importance in physics. In contrast to two-body systems three-body systems are already nonintegrable without external fields. It is beyond the scope of this article to number the numerous applications in physics, covering questions from principal atomic physics, quantum chaos up to astrophysical related applications. Several methods based on Hartree–Fock approaches [37], variational and quantum Monte Carlo [18] methods have been used to compute relevant atomic data. In strong magnetic fields helium and He-like systems become a 5-degrees-of-freedom system and all of the above mentioned methods failed in some way. Quantum Monte Carlo methods are very accurate but the necessary CPU-time [7] has to be measured in weeks to get relevant results. Therefore, this method is not

useful to produce a large set of data necessary, e.g., to simulate the observed absorption spectra of magnetic white dwarf stars. In this paragraph we will briefly describe a method based on a hyperspherical closed coupling scheme combined with Finite Elements.

The nonrelativistic Hamiltonian for two electrons in a uniform magnetic field reads

$$H = \sum_{i=0}^{2} \frac{1}{2m_i}(\boldsymbol{p}_i - e_i \boldsymbol{A}(\boldsymbol{r}_i))^2 + \sum_{i\neq j}^{2} \frac{e_i e_j}{|\boldsymbol{r}_i - \boldsymbol{r}_j|} \tag{43}$$

with m_i, e_i mass and charge of the particles, $\boldsymbol{A}$ the vector potential, 0 the label of the nucleus and $1, 2$ the two electrons. By introducing relative and centre of mass coordinates together with a Power–Zienau–Woolley transformation [38] of the wave function and neglecting the mass polarization term, the Hamiltonian [4] for the relative coordinates for the He-isoelectronic sequence in a strong magnetic field reads

$$H = \sum_{i=1}^{2} \left[-\boldsymbol{\nabla}_i^2 - \frac{2}{|\boldsymbol{r}_i|} + \beta_Z^2 (x_i^2 + y_i^2) \right] + \frac{2}{Z|\boldsymbol{r}_1 - \boldsymbol{r}_2|} + 2\beta_Z [\boldsymbol{L}_z + g_e \boldsymbol{S}_z], \tag{44}$$

where we used Z-scaled atomic units, i.e. the energy is measured in Z^2 Rydberg and the length in units of a_{Bohr}/Z, the magnetic field strength by $\beta_Z = B/(Z^2 \times 4.7010 \times 10^5\ \mathrm{T})$ and g_e is the g-factor of the electron. By appropriately rescaling the results the finite mass m_{nuc} of the nucleus can be taken into account.

Hamiltonian (44) is invariant under rotation around the z-axis and inversion with respect to the origin. Therefore, the conserved quantum numbers of the Hamiltonian are the z-component M of the total angular momentum, the parity P, the total spin S and its z-component M_S. Thus the eigenstates of the Hamiltonian can be labelled by $|PMSM_S; \nu\rangle$. However for our purpose, it is more convenient to label the states by the field free notation of helium, which is of course only correct in the asymptotic limit of vanishing magnetic fields. The connection between $|PMSM_S; \nu\rangle$ and the field-free labels is discussed in detail in [37].

Instead of the radius vectors $\boldsymbol{r}_i$ we will use Jacobi vectors

$$\boldsymbol{\xi}_1 = \frac{1}{\sqrt{2}}(\boldsymbol{r}_1 - \boldsymbol{r}_2) \tag{45}$$

and

$$\boldsymbol{\xi}_2 = \frac{1}{\sqrt{2}}(\boldsymbol{r}_1 + \boldsymbol{r}_2), \tag{46}$$

because these coordinates bear already the correct symmetry with respect to the Pauli principle. Finally we transform the coordinates to a coordinate system given by three internal coordinates and the three Eulerian angles α, β and γ, between the body and the laboratory fixed frame. As internal coordinates, we choose the hyperradius

$$R = \sqrt{\xi_1^2 + \xi_2^2}, \tag{47}$$

the hyperangle

$$\phi = \arctan\left(\frac{\xi_2}{\xi_1}\right) \tag{48}$$

and the angle u between the Jacobi coordinates $\boldsymbol{\xi}_1$ and $\boldsymbol{\xi}_2$. The body-fixed z'-axis coincides with $\boldsymbol{\xi}_1$ while $\boldsymbol{\xi}_2$ lies in the x'–z' plane. This choice simplifies considerably the symmetry requirements for

the wave function. Because this coordinates are connected to the radius vectors by an orthogonal transformation, the form of the diamagnetic Hamiltonian remains invariant.

By transforming the wave function to the standard reduced form

$$\Phi(R,\phi,u,\Omega) = R^{5/2}\sin\phi\cos\phi\,\Psi(R,\phi,u,\Omega), \tag{49}$$

where Ω are the Eulerian angles, and expanding in terms of the eigenfunctions of the symmetric top with definite parity [4] up to a maximum J-value $J_{\max}$

$$\Phi = \sum_{J=|M|}^{J_{\max}} \sum_{Q} \Phi(R,\phi,u)_{J,Q}|PJMQ\rangle_{\Omega}|SM_S\rangle, \tag{50}$$

and projecting onto the $|PJMQ\rangle_{\Omega}$ we obtain the following system of coupled partial differential equations for the functions of the internal coordinates:

$$\begin{aligned}
&\left[-\frac{\partial^2}{\partial R^2} - \frac{1}{4R^2} + H_{\mathrm{adi}}(\phi,u,R)\right]\Phi_{JQ} \\
&\quad + \frac{1}{R^2}\sum_{Q'} \frac{\langle PJMQ|2\mathrm{i}J_2|PJMQ'\rangle\partial/\partial u + \langle PJMQ|2J_1J_3|PJMQ'\rangle\,\cot u}{\cos^2\phi}\Phi_{JQ'} \\
&\quad + \beta_Z^2 R^2 \sum_{J'Q'}\left(\frac{2}{3}\delta_{JJ'}\delta_{QQ'} + \sqrt{\frac{8\pi^2}{5}}\sum_{k=0}^{2}\langle PJMQ| + 20k|PJ'MQ'\rangle\, p_k(\phi,u)\right)\Phi_{J',Q'} \\
&\quad + V_{\mathrm{para}}\Phi_{JQ} = E\Phi_{JQ}
\end{aligned} \tag{51}$$

with the adiabatic Hamiltonian

$$\begin{aligned}
H_{\mathrm{adi}}(\phi,u,R) = +\frac{1}{R^2}\Bigg(&-\frac{\partial^2}{\partial\phi^2} - \frac{1}{\sin^2\phi\cos^2\phi\sin u}\frac{\partial}{\partial u}\sin u\frac{\partial}{\partial u} \\
&+ \frac{Q^2}{\sin^2\phi\cos^2\phi\sin^2 u} - \frac{2Q^2 - J(J+1)}{\cos^2\phi} + C(\phi,u)R\Bigg)
\end{aligned} \tag{52}$$

and the paramagnetic potential

$$V_{\mathrm{para}} = 2\beta_Z[M + g_e M_S]. \tag{53}$$

The eigenfunction of Eq. (51), $\Phi_{JQ}(R,\phi,u)$, depends on the internal coordinates hyperradius R, hyperangle ϕ and Jacobi angle u. In a first attempt we tried to solve this equation by three-dimensional finite elements [6], but got serious convergency problems in strong magnetic fields. Therefore, we splitted the ansatz with three-dimensional elements into a direct product of two- and one-dimensional elements. With respect to the wave function this means that we used a further expansion of the wave function. But before splitting the wave function we have to formulate the correct boundary conditions due to the required Pauli symmetry. Interchanging the two electrons leaves the Jacobi coordinate $\boldsymbol{\xi}_2$ invariant but results in $\boldsymbol{\xi}_1 \to -\boldsymbol{\xi}_1$, and hence the hyperradius and hyperangle will be invariant under electron exchange, while

$$u \to \pi - u \quad \text{and} \quad (\alpha,\beta,\gamma) \to (\alpha+\pi, \pi-\beta, 2\pi-\gamma). \tag{54}$$

Together with the definition of the parity projected eigenfunctions of the symmetric top $|PJMQ\rangle_\Omega$ and the properties of the Wigner functions $d^J_{MM'}(\beta)$ one arrives at the following symmetry requirement:

$$\Phi_{JQ}(\phi,\pi-u,R)=P(-1)^{S+Q}\Phi_{JQ}(\phi,u,R) \tag{55}$$

and

$$\Phi_{JQ}(\phi,0,R)=0 \quad \text{for } Q>0. \tag{56}$$

Expanding the internal part of the wave function with respect to the adiabatic Hamiltonian leads to

$$\Phi_{JQ}(\phi,u,R)=\sum_\lambda f_{JQ\lambda}(R)a_{JQ\lambda}(\phi,u,R) \tag{57}$$

with $a_{JQ\lambda}(\phi,u,R)$ the adiabatic wave function which is the eigenfunction of the adiabatic Hamiltonian:

$$H_{\text{adi}}(\phi,u,R)a_{JQ\lambda}(\phi,u;R)=U_{JQ\lambda}(R)a_{JQ\lambda}(\phi,u;R). \tag{58}$$

Thus, finally we have to solve the hyperradial differential equation to get the corresponding eigenenergies and eigenfunctions

$$\begin{aligned}
&\left[-\frac{\partial^2}{\partial R^2}+U_{JQ\lambda}(R)-\frac{1}{4R^2}+2\beta_Z[M+g_eM_S]+\frac{2}{3}\beta_Z^2R^2\right]f_{JQ\lambda}(R)\\
&\quad-\sum_\mu\left[2\left\langle a_{JQ\lambda}\left|\frac{\partial}{\partial R}\right|a_{JQ'\mu}\right\rangle(R)\frac{\partial f_{JQ\mu}(R)}{\partial R}+\left\langle a_{JQ\lambda}\left|\frac{\partial^2}{\partial R^2}\right|a_{JQ'\mu}\right\rangle(R)f_{JQ\mu}(R)\right]\\
&\quad+\sum_{Q'\mu}\frac{1}{R^2}\left[\langle PJMQ|2iJ_2|PJMQ'\rangle\left\langle a_{JQ\lambda}\left|\frac{1}{\cos^2\phi}\frac{\partial}{\partial u}\right|a_{JQ'\mu}\right\rangle(R)\right.\\
&\quad\left.+\langle PJMQ|2J_1J_3|PJMQ'\rangle\left\langle a_{JQ\lambda}\left|\frac{\cot u}{\cos^2\phi}\right|a_{JQ'\mu}\right\rangle(R)f_{JQ'\mu}(R)\right]\\
&\quad+\beta_Z^2R^2\sum_{J'Q'\mu}\sum_{k=0}^{2}\sqrt{\frac{8\pi^2}{5}}\\
&\langle PJMQ|+20k|PJ'MQ'\rangle\langle a_{JQ\lambda}|p_k(\phi,u)|a_{J'Q'\mu}\rangle(R)f_{J'Q'\mu}(R)\\
&\quad=Ef_{JQ\lambda}(R).
\end{aligned} \tag{59}$$

The various matrix elements between the $|PJMQ\rangle_\Omega$ can be analytically calculated by using standard SU(2)-algebra [9]. For computing the adiabatic wave function as well as the solution of the hyperradial differential equation, we employed the method of finite elements.

The adiabatic wave function depends parametrically on the hyperradius R and explicitly on the two internal angular coordinates ϕ and u. Both angles are restricted to the interval $[0,\pi/2]$ and hence this two-dimensional space is subdivided into $n_\phi\otimes n_u$ rectangular elements. On each element the adiabatic basis function $a_{JQ\lambda}(\phi,u;R)$ is expanded in terms of biquintic splines. Application of the variational principle leads then to a generalized symmetric eigenvalue problem for the adiabatic Hamiltonian H_{adi}.

The hyperradial equation (59) is solved by subdividing the interval $[0,R_{\max}]$ for the hyperradius R in n_r quadratically spaced elements $[R_{i-1},R_i]$ according to

$$R_i=\left(\frac{i}{n_r}\right)^2R_{\max}. \tag{60}$$

Because the adiabatic wave function $a_{JQ\lambda}(\phi,u;R)$ depends parametrically on the hyperradius R, a_{JQ} is calculated on a grid in agreement with the selected nodes for solving Eq. (59). To obtain the derivatives of the adiabatic functions, a_{JQ} is in addition computed on two h and $-h$ shifted grids:

$$\frac{\partial a_{JQ\lambda}(\phi,u;R)}{\partial R} = \frac{a_{JQ\lambda}(\phi,u;R-h) - a_{JQ\lambda}(\phi,u;R+h)}{2h} + \mathrm{O}(h^3). \tag{61}$$

Again applying the method of finite elements will lead to a symmetric banded matrix for the hyperradial equation. Both eigenvalue problems have been solved by using an Arnoldi method.

2.4. Diagonalization methods

Use of discrete variable or finite element techniques maps the Hamiltonian operator onto a Hamiltonian matrix. In this paragraph we will, for the readers' convenience, add a few remarks about solving the corresponding eigenvalue problem. Of course describing the relevant program codes and the mathematical background in detail goes far beyond the size of an article. An excellent discussion of the mathematical background can be found, e.g., in [29].

The Hamiltonian matrices generated by the methods mentioned above are real, or in the case of resonances, complex symmetric matrices, which are banded and sparce. Hence the number of nonzero elements in the matrix is small compared to the total number of matrix elements. Thus, in principle we have a simple algebraic equation to determine the eigenenergies and corresponding wave functions. Nevertheless, the practical problem is still hard because the dimension of the Hamiltonian matrix is usually extremely high (from a few thousand up to a few hundred thousand). Therefore solving, e.g., the characteristic polynomial directly is numerically highly unstable and hence numerically ill-suited. Besides that the Hamiltonian matrix carries due to its huge dimension much more eigensolution than physically are converged or of interest. From this total amount of eigensolutions we are only interested in a subset. Standard library routines as provided by lapack or NAG allow only to compute either a single, extreme eigensolution or all eigensolutions. One single result is usually not sufficient, computing all eigensolution are usually not possible, because due to the large size of the matrix the necessary computer power is even to large for supercomputers. Besides this it would be a waste of CPU-time and computer space to compute thousand of unnecessary solutions simple to get the few tens or hundreds we are interested in.

Iterative methods, like the Arnoldi or Lanczos methods, suffer from the fact, that they only converge rapidly to the extreme eigenvalue. But the subset of eigenenergies which we actually want to compute might be in the centre of the total number of eigenvalues of the Hamiltonian matrix. Therefore, the first step in our computations is to map the Hamiltonian matrix onto a new matrix in which the subset of eigenenergies is mapped onto a new subset of eigenvalues of large absolute values [10]. Due to the discretization methods described above the physical system is described by a generalized eigenvalue problem

$$H\langle r_i|\psi\rangle = E\mathcal{N}\langle r_i|\psi\rangle \tag{62}$$

with H the Hamiltonian matrix, $\langle r_i|\psi\rangle$ the discretized wave function at the nodal points r_i, E the eigenenergy and $\mathcal{N}$ the normalization matrix. $\mathcal{N}$ is a symmetric matrix, hence by standard algebraic techniques this generalized eigenvalue problem can be mapped onto an ordinary eigenvalue problem. Note, that $\mathcal{N}$ remains real symmetric even in combinations with complex coordinate rotations to

compute resonances, for more details see below. By introducing a shift $\mu = E - \tilde{E}$, the generalized eigenvalue problem above can be mapped onto

$$\frac{1}{\tilde{E}}\{\mathcal{N}^t_{1/2}\langle r_i|\psi\rangle\} = \mathcal{N}^t_{1/2}(H - \mu\mathcal{N})^{-1}\mathcal{N}_{1/2}\{\mathcal{N}^t_{1/2}\langle r_i|\psi\rangle\} \tag{63}$$

with $\mathcal{N} = \mathcal{N}_{1/2}\mathcal{N}^t_{1/2}$, $1/\tilde{E}$ are the new eigenvalues and $\{\mathcal{N}^t_{1/2}\langle r_i|\psi\rangle\}$ are the transformed eigenfunctions. Hence the eigenenergies of the physical system are related to the new eigenvalues $1/\tilde{E}$ via

$$E - \mu = \tilde{E}. \tag{64}$$

Therefore, eigenenergies close to the shift μ are mapped onto eigenvalues of large absolute values by Eq. (63).

Using either an Arnoldi or a Lanzcos method we computed from Eq. (63) the eigensolutions of interest. These two methods are both iterative methods based on Krylov subspace projections [29]. The Arnoldi method is a generalization of the Lanczos process and reduces to that method for real symmetric Hamiltonian matrices. The basic idea of Krylov subspace iterations is to approximate a subset of the eigensolutions of the large Hamiltonian matrix by a much smaller matrix, where this small matrix is an orthogonal projection onto a particular Krylov subspace. Our actual computations are based either on the spectrum transformed Lanczos code from Ericsson and Ruhe [10] for real symmetric problems or on the Arnoldi codes in the ARPACK library from Lehoucq et al. [20,34]. Both packages include already all necessary computations including the spectral shift transformation. For real symmetric problems our own computations show, that the ARPACK-routines are more numerically stable but slower than the STLM-code of Ericsson and Ruhe, which is restricted to real symmetric problems. Table 1 shows some examples.

In Table 1 we compare the necessary CPU-time and computer storage for different Hamiltonian matrices obtained for the hydrogen atom by the discrete variable and finite element method. Both, the CPU-time and computer storage is measured in units of the time and space used for the Lanczos method. Hence, e.g., "1.75" in the last column means, that the Arnoldi method needed 1.75-times longer than the Lanczos method for computing the same eigenvalues of the exactly same matrix. As interpolation polynomials we took the Hermitian interpolation polynomials. Therefore the dimension N of the matrix, the number of nonzero elements M and the density of the matrix d is given by

$$\begin{aligned} N &= k_\theta(2e_r(k_\mathrm{p} - 1) + 2)), \\ M &= (2k_\mathrm{p}^2k_\theta^2 + k_\mathrm{p}k_\theta)e_r - (2k_\theta^2 + k_\theta)(e_r - 1), \\ &\Rightarrow d = \frac{2M - N}{N^2}, \\ &= \frac{e_rk_\mathrm{p}^2 - e_r + 1}{(e_rk_\mathrm{p} - e_r + 1)^2}, \end{aligned} \tag{65}$$

with k_θ the number of nodes of the θ-discretization, e_r the number of Finite Elements in the r direction and k_p the number of nodes for the hermite interpolation polynomial. Please note, that the density of the matrix becomes independent form the number of nodes of the discrete variable Θ. In the next section we will discuss some results obtained by the methods mentioned above.

Table 1
Comparison of the CPU-time and the computer space (rel. size) needed by the Lanczos and the Arnoldi code in units of the Lanczos routine. d is the density of the matrix elements and N the matrix dimension

N	Rel size	CPU-time
$d = 6.67 \times 10^{-4}$		
15,002	1.32	1.75
45,006	3.41	1.32
75,010	4.20	2.08
105,014	4.53	1.98
$d = 1.67 \times 10^{-3}$		
6,002	1.63	4.78
18,006	2.92	8.79
30,001	3.26	5.91
66,022	4.39	4.91
$d = 6.65 \times 10^{-3}$		
1,502	1.28	1.04
4,506	3.32	1.24
7,510	4.19	1.97
16,522	4.76	1.34
31,542	4.96	1.53

3. Results

In the following paragraphs we will show some results obtained for the hydrogen and alkali-metal atoms and ions in external fields. These results are of importance for astrophysical purposes, but also in solid-state physics, in low-temperature plasma physics and in quest of quantum chaos. This section will be completed by a discussion of the helium atom in strong magnetic fields relevant for magnetic white dwarf stars.

3.1. The hydrogen atom

The method we will use is based on the discrete variable method in the angular coordinates and on the finite element method with respect to the radial coordinate, as described above in detail. The discrete variable approach to the problem was introduced in [23], exploiting an idea previously used in quantum chemistry [21].

It was shown, that relativistic effects are almost negligible for the bound states of the hydrogen atom in external fields relevant for magnetic white dwarf stars [22], exempting us from the need to consider the spin explicitly in our calculations. It merely results in an energy shift proportional to the magnetic field strength. Therefore, we can restrict ourselves to the nonrelativistic Schrödinger equation. The nonseparability of the centre-of-mass motion in strong magnetic fields gives rise to an additional force perpendicular to the magnetic field axis. As this force mimics an additional homogeneous electric field and is proportional to the invariant momentum of the system, the corresponding effect is called the "Motional–Stark effect". This "centre-of-mass" problem is discussed in detail in

the literature (see e.g. [3,8,16] and references therein). For vanishing invariant momentum of the system the results for finite nuclear mass can be obtained from the calculations with infinite nuclear mass, using suitable scaling laws.

In a simple picture but with sufficient accuracy shallow donor states can often be described by a solid state analog of the hydrogen atom with rescaled energy, Bohr radius, effective charge and mass [26]. Under this assumption, the donor electron will have hydrogen-like bound states with energy

$$E_n = \frac{-\mathscr{R}}{2n^2}, \tag{66}$$

but with a Rydberg constant $\mathscr{R}$ much smaller and will to some extent show the same qualitative spectroscopic behaviour under external fields as the hydrogen atom. Therefore, studying the hydrogen atom gives also some information about shallow donor states. E.g. for the donor in GaAs the effective electron mass is 0.0665, the dielectric constant 12.56. In atomic units these two values are equal to 1. The Rydberg constant becomes 46.1 (11×10^4), the Bohr radius 9.96 nm (0.0529 nm), where the values in brackets are the corresponding hydrogen values. Hence an electric field of about 10^{10} V/m will have the same impact on a H-atom as a field of 2×10^4 V/m on a donor.

3.1.1. The hydrogen atom in strong external fields

The Hamiltonian of a hydrogen atom with infinite nuclear mass in an external magnetic field $\boldsymbol{B}$ and electric field $\boldsymbol{F}$ reads

$$H = \underbrace{\frac{|\boldsymbol{p}|^2}{2m_e}}_{\text{kin.}} - \underbrace{\frac{e^2}{|\boldsymbol{r}|}}_{\text{Coul.}} + \underbrace{\frac{e}{2m_e}\boldsymbol{B}\cdot\boldsymbol{L}}_{\text{paramagn.}} + \underbrace{\frac{e^2}{8m_e}(\boldsymbol{B}\times\boldsymbol{r})^2}_{\text{diamagn.}} + \underbrace{e\boldsymbol{F}\cdot\boldsymbol{r}}_{\text{electr.}}. \tag{67}$$

Using atomic units, we measure energies in units of the Hartree energy $E_H = \alpha^2 m_e c^2 \approx 27.21$ eV, the magnetic field strength $\beta = B/B_0$ in units of $B_0 = 2\alpha^2 m_e^2 c^2/e\hbar \approx 4.701 \times 10^5$ T, the electric field strength $\Phi = F/F_0$ in units of $F_0 = \alpha^3 m_e^2 c^3/e\hbar \approx 5.14 \times 10^{11}$ V/m and lengths in units of the Bohr radius $a_B = \hbar/\alpha m_e c \approx 0.53 \times 10^{-10}$ m. Then the Hamiltonian (67) becomes (in spherical coordinates r, ϑ and φ, with the magnetic field axis pointing in the $z = r\cos\vartheta$ direction and δ representing the angle between the two external fields):

$$H(r,\vartheta,\varphi) = -\frac{1}{2r^2}\frac{\partial}{\partial r}r^2\frac{\partial}{\partial r} + \frac{1}{2r^2}L^2(\vartheta,\varphi) - \mathrm{i}\beta\frac{\partial}{\partial\varphi} + U(r,\vartheta,\varphi), \tag{68}$$

where

$$L^2(\vartheta,\varphi) = -\frac{1}{\sin\vartheta}\left(\frac{\partial}{\partial\vartheta}\sin\vartheta\frac{\partial}{\partial\vartheta} + \frac{1}{\sin\vartheta}\frac{\partial^2}{\partial\varphi^2}\right), \tag{69}$$

$$U(r,\vartheta,\varphi) = -\frac{1}{r} + \frac{1}{2}\beta^2 r^2\sin^2\vartheta + \Phi r(\cos\vartheta\cos\delta + \sin\vartheta\cos\varphi\sin\delta). \tag{70}$$

For vanishing electric field strength, $\Phi = 0$, the spherical symmetry of the hydrogen atom is broken by the diamagnetic contribution of the strong magnetic field $\beta^2 r^2\sin^2\theta$ to the total potential. The quantum number m and the z-parity, π_z, are conserved. For parallel magnetic and electric fields, $\delta = 0$, the quantum number m is still conserved, but not the parity π_z. Therefore, in this two cases we have to solve a $(2 \oplus 1)$-dimensional system. For perpendicular fields, $\delta = \pi/2$, the rotational

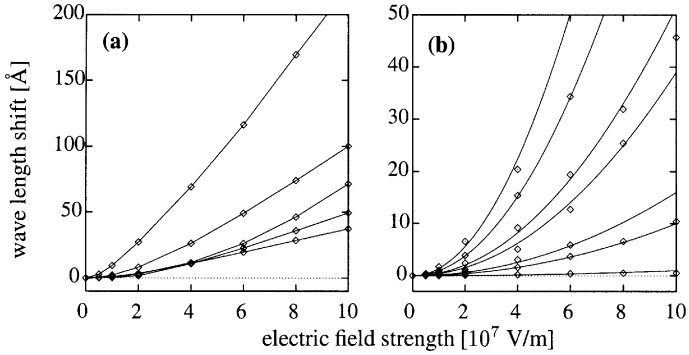

Fig. 2. Absolute value of the shift of the wave length as a function of the electric field strength for the stationary components of Balmer β. The calculated values are represented by squares, the solid lines are interpolated quadratic functions. On the left-hand side (a) for those transitions with small stationary magnetic field ($\beta < 0.02$) and on the right-hand side (b) with strong stationary magnetic field ($\beta > 0.02$).

symmetry with respect to the z-axis is broken, hence m is no longer conserved, which results in a three-dimensional system. In this case the z-parity, π_z, is conserved, but for arbitrary relative angles δ (unequal 0 or $\pi/2$) between the magnetic and electric field axis no discrete symmetry is left and hence neither m nor π_z are conserved quantities.

The identification of stationary lines (transitions whose wavelength run through an extrema as a function of the magnetic field strengths) has been the most striking application of atomic data to the spectra of magnetized white dwarf stars. In [12] we investigated the stationary lines of the hydrogen atom in external magnetic and electric fields relevant to white dwarf stars, by calculating the magnetic field strengths, the wavelengths and the oscillator strengths of the extrema of all stationary components of the Lyman α, the Balmer α and the Balmer β transitions. By this computations we could show, that the Lyman α transitions are rather insensitive to the electric field, whereas the electric field exerts a considerable influence on the Balmer transitions. Moreover, further stationary components compared to the pure diamagnetic case occur, caused by the symmetry break due to the additional electric field. In most cases the relevant oscillator strength remain small compared to transitions already allowed without additional electric fields. Computed atomic data for various electric and magnetic field strengths can be obtained on request, but will not be published here due to the lack of space. Some relevant examples are shown in [11,12]. (We plan to publish the huge data set already available via WWW.) As an example for the effect of additional electric fields to the magnetic field we will briefly discuss the Balmer β transition.

Out of the 26 Balmer β transitions allowed in the diamagnetic case, seven transitions exhibit stationary behaviour, with altogether 14 extrema in the magnetic field range relevant for magnetic white dwarf stars. As an example we show in Fig. 2 the absolute shift of the wave length as a function of the electric field strength for these stationary Balmer β components in parallel magnetic and electric fields. For two of the transitions the oscillator strength becomes extremely small in very strong electric fields, and therefore are not plotted in the figure. A table of the values can be found in [12]. In contrast to the Balmer α lines the Balmer β transitions are much more influenced by external electric fields and show as the Balmer α transitions, wave length shifts as well to the blue and to

the red. In addition to these stationary components of the Balmer β transitions 5 more stationary Balmer β transitions become allowed in parallel magnetic and electric fields, with altogether six new extrema.

The single electron of the hydrogen atom in external fields is, of course, a fermion and the Pauli exclusion principle holds. Hence, there are no atomic states which share the same quantum number, and therefore only those states can be degenerate (have the same energy) which can be labelled by a quantum observable with different values. For the hydrogen atom in parallel electric and magnetic fields the symmetry with respect to reflection on the xy-plane is broken by the electric field and hence the z-parity π_z is no longer conserved. As pointed out above states could be degenerate with respect to the energy for vanishing electric fields. For a small nonvanishing electric field the degeneracy is broken and hence level-crossing becomes forbidden, which can be observed as avoided crossings. One important aspect is the behaviour of the eigenstates. In case of an allowed level-crossing the wave functions run without any distortion through this point of crossing. For an avoided crossing the two neighbouring wave functions are interacting with each other, which leads to the observed repelling character of an avoided crossing. Far away from the point of the avoided crossing the wave functions are similar to the ones without an additional electric field. Close to the energy value at which the avoided crossing occurs, both wave functions are distorted and mixed with each other. An example for this behaviour can be found in [32].

3.1.2. Van-der-Waals interaction

The Hamiltonian of the hydrogen atom in front of a metal surface reads in semiparabolic coordinates ($\sqrt{(x^2+y^2)}=\mu\nu$, $z=\frac{1}{2}(\mu^2-\nu^2)$)

$$H(\mu,\nu,p_\mu,p_\nu)=\frac{1}{2}\frac{p_\mu^2+p_\nu^2}{(\mu^2+\nu^2)}+V_{ms} \tag{71}$$

with

$$V_{ms}=-\frac{1}{2d}-\frac{4}{\mu^2+\nu^2}+\frac{2}{\sqrt{\mu^2\nu^2+(2d+\frac{1}{2}(\mu^2\nu^2))}}-\frac{1}{2(d+\frac{1}{2}(\mu^2-\nu^2))} \tag{72}$$

and d the distance from the metal surface. In radial coordinates the nodes of the wave function are quadratically spaced, whereas in semiparabolic coordinates the nodes are approximately equally spaced and the characteristic dimension are equal in μ and ν direction. Note, that this would not be true, e.g., for cylindrical coordinates ρ and z. Therefore, by representing Coulomb-like potentials in semiparabolic coordinates finite elements of constant dimension are already optimally spaced. By expanding the Hamiltonian with respect to the distance d, Ganesan and Taylor [14] calculated Rydberg eigenstates and eigenvalues in a Sturmian basis. Such an expansion is unnecessary for a two-dimensional finite element approach. To solve this problem we used two-dimensional finite elements with quadratic and cubic form-functions. For more details of higher-dimensional finite elements see, e.g., the excellent book of Akin [2]. In Fig. 3 we show as an example the 25th eigenfunction of a hydrogen atom placed in a distance of 50 Å in front of a metal surface. Basis set calculations would necessitate huge Taylor expansions in the Hamiltonian potential leading to serious convergency problems. Hence finite element techniques for quantum systems are especially useful for computations in such extreme situations, where the Hamiltonian is far from integrable limits, but the wave functions are still not too much structured.

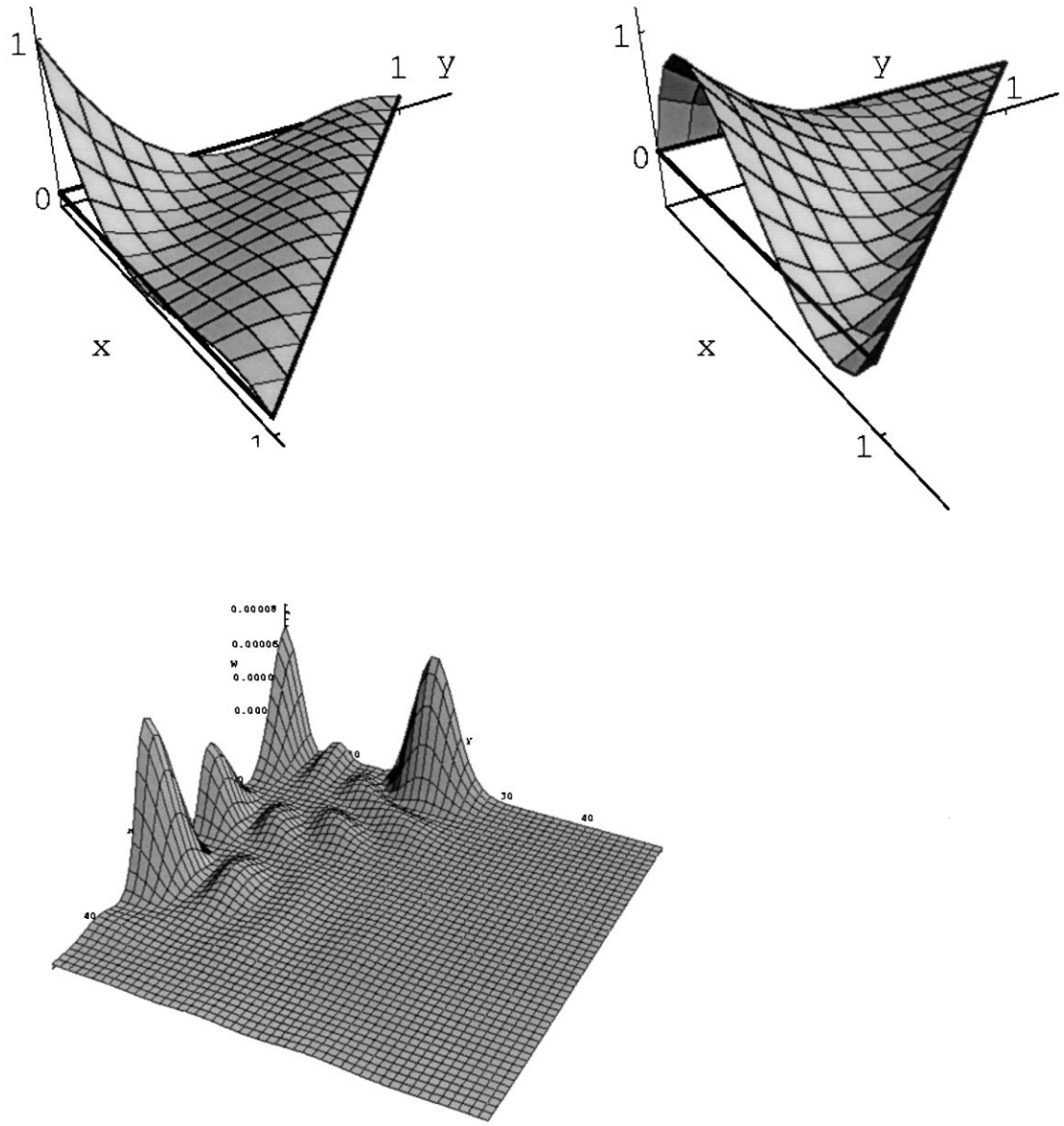

Fig. 3. This figure shows as an example on top cubic form-functions used for the finite element calculations and the 25th $m = 0$ eigenstate of the hydrogen atom localized in front of a metal surface in a distance of 50 Å.

3.1.3. Resonances

Due to the external electric fields the ionization threshold of the atom is lowered from the field-free value. In fact, all states become quasi-bound, as the electron can ionize by tunneling through the potential states. This process becomes important for states close to the classical ionization energy or above. The combination of the complex coordinate method with an *R*-matrix quantum-defect method

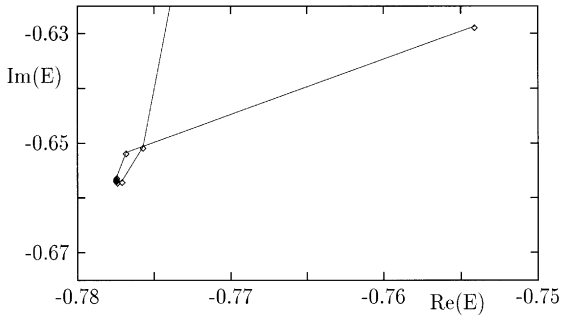

Fig. 4. Complex energy of the hydrogen ground state for $F = 0.3$ as a function of the complex rotation angle Θ. To uncover the "convergence trajectory" the deviation from the converged value is plotted: $\mathrm{Re}(E) = (E_R + 0.596722) \times 10^6$ and $\mathrm{Im}(E) = (\Gamma/2 + 0.1306655) \times 10^7$, with E_R the real part of the complex energy eigenvalue and Γ the FWHM of the resonance.

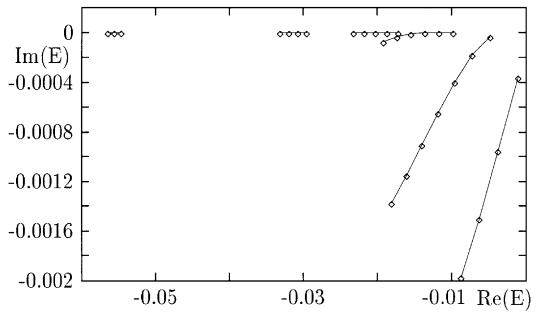

Fig. 5. Complex eigenenergies of the hydrogen atom for magnetic quantum number $m = 0$ at an electric field $F = 0.0001$ in atomic units. The classical ionization threshold is $\mathrm{Re}(E) = -0.02$.

is discussed for parallel magnetic and electric fields for hydrogen under astrophysical quest in [30] and for sodium atoms (in general nonhydrogenic Rydberg atoms) for laboratory field strengths in [31]. Of course complex coordinate rotations can be also combined with discrete variable and finite element techniques. Some results are presented in Figs. 4 and 5. In contrast to bound states the Hamiltonian matrix becomes complex symmetric, but the normalization matrix $\mathcal{N}$ remains real. Therefore, we have to solve a complex symmetric eigenvalue problem, Eq. (62).

In the complex coordinate method the real configuration space coordinates are transformed by a complex dilatation. The Hamiltonian of the system is thus continued into the complex plane. This has the effect that, according to the boundaries of the representation, complex resonances are uncovered with square-integrable wave functions and hence the space boundary conditions remain simple. This square integrability is achieved through an additional exponentially decreasing term

$$r \to r \exp(\mathrm{i}\Theta). \tag{73}$$

After the coordinates entering the Hamiltonian have been transformed, the Hamiltonian is no longer hermitian and thus can support complex eigenenergies associated with decaying states. The spectrum of a complex-rotated Hamiltonian has the following features [17]: Its bound spectrum remains

unchanged, but continuous spectra are rotated about their thresholds into the complex plane by an angle of -2Θ. Resonances are uncovered by the rotated continuum spectra with complex eigenvalues and square-integrable (complex rotated) eigenfunctions.

In the Stark effect the whole real energy axis is the continuum spectrum and no threshold exists in the unrotated Hamiltonian for the continuous spectrum to rotate about. The Hamiltonian for the hydrogen atom in parallel electric and magnetic fields, after the above complex transformation has been applied, becomes

$$H(\Theta) = -\exp(-2\mathrm{i}\Theta)\frac{\nabla^2}{2} - \exp(-\mathrm{i}\Theta)\frac{1}{r} + \frac{1}{2}\gamma(l_z + 2s_z) + \exp(2\mathrm{i}\Theta)\frac{1}{8}\gamma^2 r^2 \sin^2\theta + \exp(\mathrm{i}\Theta)Fr\cos\theta, \tag{74}$$

using atomic units and spherical coordinates.

We calculated photoionization spectra [30] at optical wavelengths in a strong magnetic field with parallel electric fields of various strengths. The electric field modulates the ionization spectra strongly through an onsetting resonance structure which behaves smoothly by changing the electric field strength. The electric fields in the atmosphere of the white dwarf are generated by free electrons and ions in the stellar plasma and hence distributed statistically. Taking this statistical origin into account the strong resonance features are smeared out by the electric field distribution and the opacities can be approximated by straight lines over the relatively small wave length range in question.

In Fig. 4 we show an example for the convergence to a complex eigenvalue as function of the complex angle Θ. Convergence to a complex eigenvalue is systematic and follows a pattern with an accumulation point at the correct complex value. Fig. 5 shows hydrogen resonances for an electric field strength of $F=0.0001$ just around the classical ionization threshold. The widths of the resonances below the ionization threshold is relatively small. The single n-manifolds are well separated in the complex plane. A resonance belonging to a certain n-manifold which lies lower on the real axis has a bigger imaginary part of energy than one of higher energy. This astonishing behaviour is due to the fact, that the corresponding wave function and hence the probability of presence of the valence electron is localized further in the direction of the anode of the electric field and thus tends to ionize more easily.

3.2. Alkali systems

The combination of the discrete variable with the finite element method allows not only to compute atomic data for the hydrogen atom. Atomic data for alkali-metal atoms and alkali-like ions can be obtained by a suitable phenomenological potential, which mimics the multielectron core. The basic idea of model potentials is to represent the influence between the nonhydrogenic multielectron core and the valence electron by a semi-empirical extension to the Coulomb term, which results in an analytical potential function. The influence of the nonhydrogenic core on the outer electron is represented by an exponential extension to the Coulomb term [15]:

$$V(r) = -\frac{e^2}{r}\{\tilde{Z} + (Z - \tilde{Z})\exp(-a_1 r) + a_2 r\exp(-a_3 r)\}. \tag{75}$$

Z is the nuclear charge, $\tilde{Z}$ the ionization stage. (For neutral atoms the ionization stage is $\tilde{Z} = 1$, for single ionized atoms $\tilde{Z} = 2$, and for multi-ionized atoms $A^{(n+)}\tilde{Z} = n + 1$.) The coefficients a_i

Table 2
Atomic data for Li states of principle quantum $n=2,\ldots,7$ compared with experimental data and various other numerical computations. (μ_l is the quantum defect, energies in Hartree)

State	Energy	μ_l	μ_l^1	μ_l^2	μ_l^3
2s	−0.197331	0.40820	0.40946	0.41153	0.41070
2p	−0.130068	0.03935	0.03916	0.04069	0.04049
3s	−7.412388E-02	0.40280	0.40165	0.40392	0.40455
3p	−5.724192E-02	0.04452	0.04271	0.04445	0.04453
3d	−5.557495E-02	0.00052	0.00097	0.00147	0.00161
4s	−3.860689E-02	0.40124	0.39953	0.40178	0.40281
4p	−3.198441E-02	0.04619	0.04385	0.04567	0.04587
4d	−3.126147E-02	0.00073	0.00125	0.00167	0.00186
4f	−3.125008E-02	0.00000	—	0.00000*	—
5s	−2.363552E-02	0.40059	0.39864	0.40089	0.40209
5p	−2.038076E-02	0.04693	0.04435	0.04622	0.04648
5d	−2.000664E-02	0.00083	0.00138	0.00177	0.00199
5f	−2.000007E-02	0.00000	—	0.00000*	—
5g	−2.000000E-02	0.00000	—	0.00000*	—
6s	−1.594531E-02	0.40025	0.39819	0.40043	0.40172
6p	−1.411061E-02	0.04733	0.04462	0.04652	0.04680
6d	−1.389300E-02	0.00089	0.00145	0.00182	0.00205
6f	−1.388895E-02	0.00001	—	0.00000*	—
6g-h	−1.388890E-02	0.00000	—	0.00000*	—

are optimized numerically so as to reproduce the experimental field-free energy levels and hence quantum defects of the alkali-metal atom or alkali-like ion. (A complete list of parameters a_i for all alkali-metal atoms and the Li isoelectronic sequence is published in [33].) The total interaction for vanishing external fields holds the following properties:

$$\lim_{r\to 0} V(r) = \lim_{r\to 0}\left\{-\frac{Ze^2}{r}\right\} \tag{76}$$

and

$$\lim_{r\to \infty} V(r) = \lim_{r\to \infty}\left\{-\frac{\tilde{Z}e^2}{r}\right\}. \tag{77}$$

Model potential studies combined with discretization techniques allow even on small computers quick parameter studies of effective single-electron ions and atoms. These model potentials are restricted to those energy regions where it is sufficient to treat the excitation of the valence electron isolated from the ionic core, which means no additional core excitations and no additional electron excitations are allowed.

In Tables 2 and 3 we compare our results with those obtained by ab initio close-coupling calculations [25] in column 4 (μ_l^1), with experimental data (if available) in column 5 (μ_l^2), and with results obtained by model potential calculations of the "opacity group" [25] in the last column for Li and C IV. The model potential parameters are listed in Table 4. The model potential used by the

Table 3
Atomic data for Li-like carbon (CIV) for $n = 2, \ldots, 7$ (μ_l is the quantum defect, energies in Hartree)

State	Energy	μ_l of V(r)	μ_l^1	μ_l^2	μ_l^3
2s	−2.363446	0.16019	0.16190	0.16282	0.16191
2p	−2.073926	0.03597	0.03597	0.03698	0.03618
3s	−0.989626	0.15679	0.15668	0.15770	0.15826
3p	−0.911855	0.03802	0.03674	0.03792	0.03833
3d	−0.889756	0.00146	0.00142	0.00162	0.00181
4s	−0.541327	0.15572	0.15513	0.15615	0.15712
4p	−0.509797	0.03862	0.03700	0.03818	0.03899
4d	−0.500488	0.00195	0.00172	0.00194	0.00222
4f	−0.500007	0.00003	—	0.00000*	—
5s	−0.340837	0.15525	0.15449	0.15547	0.15663
5p	−0.325036	0.03889	0.03714	0.03828	0.03928
5d	−0.320279	0.00218	0.00187	0.00210	0.00240
5f	−0.320006	0.00005	—	0.00000*	—
5g	−0.320000	0.00000	—	0.00000*	—
6s	−0.234164	0.15500	0.15407	0.15512	0.15636
6p	−0.225141	0.03902	0.03715	0.03835	0.03943
6d	−0.222392	0.00230	0.00199	0.00222	0.00251
6f	−0.222226	0.00006	—	0.00000*	—
6g-h	−0.222222	0.00000	—	0.00000*	—

Table 4
Some potential parameter for the model potential Eq. (75). $\overline{\Delta E/E}$ is the averaged relative error computed over all eigenstates with principle quantum number $n \leqslant 10$ with ΔE the difference between our computation and the experimental results

Ion	Z	$\tilde{Z}$	a_1	a_2	a_3	$\overline{\Delta E/E}$
Li I	3	1	3.395	3.212	3.207	0.00007
C IV	6	4	7.655	7.654	7.674	0.00036
Ne VIII	10	8	13.246	12.941	13.341	0.00025

opacity group differs from ours:

$$V(r) = -\frac{z}{r} - \frac{2}{r}(1 + \delta x + \mathrm{d}'x^2)\exp(-\gamma x) - \frac{\alpha_d}{2r^4} g_2(\beta x), \tag{78}$$

where the Greek letters are fit parameters, $z = (Z - 2)$ is the net charge of the atomic core, $x = zr$ and

$$g_2(y) = \chi_2(y)^2, \qquad \chi_2(y) = 1 - \exp(y)\sum_{n=0}^{2} \frac{y^n}{n!}. \tag{79}$$

Despite the fact that the model potential, Eq. (78), depends on more parameters the results are not better, and the additional $1/r^4$-singularity makes discretization computations much harder compared

Table 5
Comparison of the oscillator strengths obtained at zero field with those of [36]

	$\Delta M = 0,\ \beta_Z = 0$	
	This work	Tang et al.
$2^1P_0 \rightarrow 1^1S_0$	0.267	0.276
$3^1P_0 \rightarrow 2^1S_0$	0.144	0.149
$2^1P_0 \rightarrow 2^1S_0$	0.423	0.377
$3^1P_0 \rightarrow 1^1S_0$	0.070	0.074

to our model potential, Eq. (75). For large angular momenta no literature values are available. Therefore we added for the readers' convenience 0.00000^* in the column with the results obtained by close-coupling computations. This is justified as the quantum defect is close to zero for higher angular momenta.

By combining the model potential technique with discretization methods and complex coordinate rotations resonances can be easily uncovered. As an example we studied some transitions for Li-like nitrogen. Due to the observed shift of various transitions these results could be used to obtain some information about the microelectric fields in low-temperature plasmas, which are connected with the electron density. Relative strengths between various transitions should allow to get some information, e.g., about the temperature of the plasma. This data-set will be published elsewhere. In quest of astrophysical observations of an Am-Her-system we computed also Li-like Ne in intense magnetic fields. These computations allowed to interpret the observed absorption structure. (Details will be published elsewhere.) Hence in conclusion model potential-based computations are useful to study the contribution and importance of alkali metal atoms and alkali-like ions in a plasma environment.

3.3. The helium atom

In the last paragraph we will show some results for the helium atom in intensive magnetic fields obtained by the method described above. These computations were motivated by still unexplained observed absorption structures in spectra of magnetic white dwarf stars, like the GD229, for which transitions of neutral He are considered to be important. Therefore the properties of the helium atom in strong magnetic fields are of great relevance.

To test the reliability of our method we compared our energies against the numerically exact results for field-free nonrelativistic helium by [1]. The agreement is good to very good for the *S*-states while fair for the *P*-states. Thus one can expect our wavelengths to be accurate to about 1%. Considering the strong variation of the magnetic field within a neutron or white dwarf star due to the dipole or even higher multipole field assumed, this accuracy should be sufficient for a reliable calculation of model-spectra. As a further, more sensitive test of our numerical method we also checked our results for oscillator strengths at zero field. In Table 5 we show our results for the oscillator strengths at zero field. We also give those obtained by [36]. It is seen that the agreement is fair to good except for $2^1P_0 \rightarrow 2^1S_0$ which is due to the small energy difference involved. However, the corresponding wavelength is very large and thus unimportant for astrophysical applications.

We have calculated the wavelengths of dipole transitions between a number of singulett- as well as triplett-states for $\beta_Z \leqslant 0.1$, i.e. for field strengths up to 1.88×10^5 T. Some results have been published in [5]. Due to the lack of space we cannot label all these results here, and hence we will provide these data via WWW. But, e.g., between singlet states with $\Delta M = -1$, the wavelengths vary by approximately a factor of 2. We also found some transitions exhibit wavelength extrema translating into stationary lines, which should be observable as prominent structures in the photoabsorption spectra of white dwarf stars. The computed extrema cover the whole wave length range, from the ultraviolet up to the infrared area. E.g. for the transition $3^1P_1 \rightarrow 2^1S$ we found a maximum at $\beta_Z \approx 0.008$, $\lambda \approx 4820$ Å, for $4^1P_1 \rightarrow 3^1S$ a maximum at $\beta_Z \approx 0.018, \lambda \approx 7730$ Å and a weak minimum for $\beta_Z \approx 0.072, \lambda \approx 5750$ Å, and for $5^1P_1 \rightarrow 3^1S$ a maximum at $\beta_Z \approx 0.016, \lambda \approx 2250$ Å and again a minimum at about $\beta_Z \approx 0.078, \lambda \approx 770$ Å to label only a few. A more complete list is in preparation and will be published elsewhere.

4. Conclusion

Discrete variable techniques and finite element methods, if necessary combined with additional model-dependent numerical techniques, turned out to be a useful, quick and accurate way for studying nonintegrable quantum system. By this methods we were able to calculate atomic properties under physical situations in which other methods, like basis set expansions or a perturbative treatment, failed. The basic idea of this computation is graphically condensed in Fig. 6.

By a combination of the discrete variable with the finite element method we were able to compute atomic data for the hydrogen atom in white dwarf or neutron star fields. With suitable phenomenological potentials, which mimic analytically alkali core effects, atomic data are obtained which have

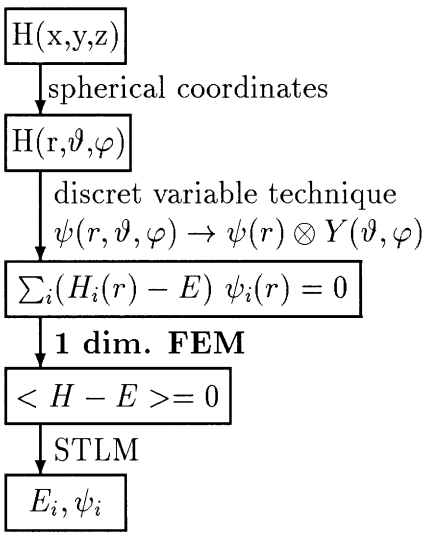

Fig. 6. Graphical picture of our "working horse", where "FEM" stands for "finite element method" and "STLM" for spectrum transformed Lanczos method.

the same accuracy as those computed by (the more CPU-time consuming) *R*-Matrix quantum defect methods. In addition time-dependent problems can be easily solved by time discretizations, like the Cayley method [13] and complex coordinate rotations allow to uncover resonances or scattering states.

One advantage of discretization techniques, not mentioned yet, is its broad approach. For basis set expansions an optimized basis have to be selected in order to get a simple treatable numerical problem. For discretization techniques the potential is not so important. Quite different potentials can be treated, simply by "cut and paste" of the potential-function under consideration. This opens the door for a quick treatment of quite different systems without the necessity to derive always new computational techniques and hence to concentrate on the physical and not the numerical problem.

The last presented example was the combination of close-coupling ideas with finite element techniques. By merging these two ideas we were able — for the first time — to obtain sufficiently accurate atomic helium data in strong magnetic fields. The results shown above are the first step but the method has to be improved further to reduce the necessary CPU-time and to improve the accuracy. One additional important step will be to include adaptive techniques, to improve the accuracy without enlarging the finite element space too much.

Finally, not only under scientific, but also under pedagogical aspects discretizations techniques are of interest. With the availability of powerful low-cost computers students have the possibility to use this more advanced numerical techniques to study quantum systems, and hence courses on quantum mechanics and the necessary exercises are no longer restricted to the perturbative and ground state "pencil-regime" of quantum dynamical systems.

Acknowledgements

W.S. thanks Prof. H. Ruder for his encouragement, R. G.-F. and M. B. for the kind hospitality at the Lehrstuhl für Theoretische Astrophysik.

This work was supported by the Deutsche Forschungsgemeinschaft (DFG), the Deutscher Akademischer Austauschdienst (DAAD), the Foundation for Research Development (FRD) of South Africa, and has been partially supported by the Spanish DGES project No. PB95-1205 and by the Junta de Andalucia under grant FQM-207.

References

[1] Y. Accad, C.L. Pekeris, B. Schiff, S and P states of the helium ioselectronic sequence up to $Z = 10$, Phys. Rev. A 4 (1971) 516 –536.

[2] J.E. Akin, Finite Elements for Analysis and Design, Academic Press, London, 1998.

[3] D. Baye, N. Clerbaux, M. Vincke, Delocalized states of atomic hydrogen in crossed electric and magnetic fields, Phys. Lett. A 166 (1992) 135–139.

[4] M. Braun, Anwendung der Methode der finiten Elemente auf das Zwei-Elektronen-Problem in starken Magnetfeldern, Thesis, Tübingen, 1993.

[5] M. Braun, H. Elster, W. Schweizer, Hyperspherical close coupling calculations for helium in a strong magnetic field, Phys. Rev. A 57 (1998) 3739.

[6] M. Braun, W. Schweizer, H. Herold, Finite-element calculations for S-states of helium, Phys. Rev. A 48 (1993) 1916–1920.

[7] D.M. Ceperley, privat communication, 1997.
[8] O. Dippel, P. Schmelcher, L.S. Cederbaum, Charged anisotropic harmonic oscillator and the hydrogen atom in crossed electric and magnetic fields, Phys. Rev. A 49 (1994) 4415–4429.
[9] A. Edmonds, Angular Momentum in Quantum Mechanics, Princeton Univ. Press, Princeton, 1974.
[10] T. Ericsson, A. Ruhe, The spectral transformation Lanczos method for the numerical solution of large sparse generalized symmetric eigenvalues problems, Math. Comput. 35 (1980) 1251–1268.
[11] P. Fassbinder, W. Schweizer, Hydrogen atom in very strong magnetic and electric fields, Phys. Rev. A 53 (1996) 2135–2139.
[12] P. Fassbinder, W. Schweizer, Stationary hydrogen lines in magnetic and electric fields of white dwarf stars, Astron. Astrophys. 314 (1996) 700–706.
[13] P. Fassbinder, W. Schweizer, T. Uzer, Numerical simulation of electronic wavepacket evolution, Phys. Rev. A 56 (1997) 3626–3633.
[14] K. Ganesan, K.T. Taylor, Rydberg states of the hydrogen atom near a metal surface, J. Phys. B 29 (1996) 1293–1306.
[15] J. Hannsen, R. McCarrol, P. Valiron, Model potential calculations of the Na–He system, J. Phys. B 12 (1979) 899–908.
[16] H. Herold, H. Ruder, G. Wunner, The two-body problem in the presence of a homogeneous magnetic field, J. Phys. B 14 (1981) 751–764.
[17] Y.K. Ho, The method of complex coordinate rotation, Phys. Rep. 99 (1983) 1–68.
[18] M.D. Jones, G. Ortiz, D.M. Ceperley, Released-phase quantum Monte Carlo method, Phys. Rev. E 54 (1996) 6202–6210.
[19] D.M. Larsen, Inhomogeneous broadening of Lyman-series absorption of simple hydrogenic donors, Phys. Rev. B 13 (1976) 1681–1691.
[20] R.B. Lehoucq, D.C. Sorenson, C. Yang, Solution of large scale eigenvalue problems with implicitly restarted Arnoldi methods, ARPACK users' guide; 1997.
[21] J.C. Light, I.P. Hamilton, J.V. Lill, Generalized discrete variable approximation in quantum mechanics, J. Chem. Phys. 82 (1985) 1400–1409.
[22] K.A.U. Lindgren, J.T. Virtamo, Relativistic hydrogen atoms in a strong magnetic field, J. Phys. B 12 (1979) 3465–3472.
[23] V.S. Melezhik, Three-dimensional hydrogen atom in crossed magnetic and electric fields, Phys. Rev. A 48 (1993) 4528–4538.
[24] W. Miller, Lie Theory and Special Functions, Academic Press, New York, 1968.
[25] G. Peach, H.E. Saraph, M.J. Seaton, Atomic data for opacity calculations IX: The Li-isoelectronic sequence, J. Phys. B 21 (1988) 3669–3683.
[26] A.K. Ramdas, S. Rodriguez, Spectroscopy of the solid-state analogues of the hydrogen atom: donors and acceptors in semiconductors, Rep. Prog. Phys. 44 (1981) 1297–1387.
[27] L.R. Ram-Mohan, S. Saigal, D. Dossa, J. Shertzer, The finite-element method for energy eigenvalues of quantum mechanical systems, Comput. Phys. 1 (1990) 50–59.
[28] P. Ring, P. Schuck, The Nuclear Many-Body Problem, Springer, Berlin, 1980.
[29] Y. Saad, Numerical Methods for Large Eigenvalues Problems: Theory and Algorithms, Wiley, New York, 1992.
[30] I. Seipp, W. Schweizer, Electric fields for hydrogen bound-free transitions in magnetic white dwarfs, Astron Astrophys. 318 (1997) 990–996.
[31] I. Seipp, K.T. Taylor, W. Schweizer, Atomic resonances in parallel electric and magnetic fields, J. Phys. B 29 (1996) 1–13.
[32] W. Schweizer, P. Fassbinder, The discrete variable method for non-integrable quantum systems, Comput. Phys. 11 (1997) 641–647.
[33] W. Schweizer, P. Fassbinder, R. González-Feréz, Model potentials for alkali metal atoms and alkali-like ions, At. Data Nucl. Data Tables 72 (1999), in press.
[34] D.C. Sorensen, Implicit application of polynomial filters in a k-step Arnoldi method, SIAM J. Mater. Anal. Appl. 13 (1992) 357–385.
[35] G. Szegö, Orthogonal Polynomials, College Publication rev, American Mathematical Society, Providence, RI, 1959.

[36] J. Tang, S. Wanatabe, M. Matsuzawa, Dipole density function and evaluation of the oscillator strengths of He, Phys. Rev. A 46 (1992) 3758–3761.
[37] G. Thurner, H. Körbel, M. Braun, H. Herold, R. Ruder, G. Wunner, Hartree–Fock calculations for excited states of two-electron systems in strong magnetic fields, J. Phys. B 26 (1993) 4719–4750.
[38] R.G. Woolley, Molecular quantum dynamics, Proc. Roy. Soc. London A 321 (1971) 557–572.
[39] G. Wunner, W. Schweizer, H. Ruder, Hydrogen atoms in strong magnetic fields — in the Cosmos and in the Laboratory, in: The Hydrogen Atom, F. Bassani, M. Ingusico, T. Hänsch (Eds.), Springer, Berlin, 1989, pp. 300–310.